Progress in Organic Coatings 174 (2023) 107287

Contents lists available at ScienceDirect

Progress in Organic Coatings

journal homepage: www.elsevier.com/locate/porgcoat

Halloysites as carriers for Ce(III) and La(III) ions in anti-corrosivepaint for steel

S. Roselli [a], M. Revuelta [b,c], C. Deya [a,c,*], R. Romagnol [a,1]

[a] Facultad de Ingeniería, UNLP, Argentina
[b] Facultad de Ciencias Exactas, UNLP, Argentina
[c] CIDEPINT (CONICET-CICPBA-Ing.UNLP), Av. 52 e/ 121 y 122 sin n°, La Plata B1900AYB, Argentina

ARTICLE INFO

Keywords:
Halloysite
Rare earths ions
Steel
Corrosion
Paint
Electrochemical tests
Accelerated tests

ABSTRACT

Aluminosilicates minerals are used as inhibitive cation carriers to protect metals from corrosion. The objective of this paper was to study the anticorrosive behaviour of natural halloysite, loaded with ions Ce(III) or La(III), as carrier pigment to inhibit steel corrosion. The mineral was characterized by Fourier transform infra-red spectroscopy and x-ray diffraction. Steel in contact with the loaded mineral and immersed in NaCl 0.05 M solution was study by electrochemical tests, scanning electron microscopy and energy dispersive x-ray analysis. Besides alkyd solvent paints were formulated, prepared, and tested (salt spray and humidity chambers exposure and electrochemical tests) employing the loaded halloysite together with or without zinc phosphate. Results showed that the protective action of the paints applied on SAE 1010 steel depends on the loaded cation and on the environment to which they were exposed.

1. Introduction

Mild steel is commonly used in industrials and in the manufacturing of equipment for most industries around the world. It is cheaper compared with other metals and its durable, hard and easy-to-wear physical properties make it a major choice in the manufacture of equipment parts. The main problem through the uses of mild steel in industry is its resistance against corrosion, especially if it is exposed to aggressive environments. This leads to increases in company costs due to maintenance of equipment using steel. So, organic coatings containing corrosion inhibitors are commonly used to protect it against corrosion.

Traditional anticorrosive pigments employed in paints were chromate and lead based salts. However, due to health and environmental concern about them, zinc phosphate and related compounds were incorporated as replacements. Phosphate-based anticorrosive pigments are also being questioned because the anion causes eutrophication in freshwater reservoirs [1]. In addition, some of them have heavy cations, such as zinc or strontium, whose use has also been restricted. Modified siliceous materials were suggested to eliminate chromates and reduce the phosphate content due to their ability to exchange either passivating anions or cations. The most common anion exchange pigment is hydrotalcite modified with vanadate which proved to be effective in restraining steel corrosion but it is not as effective as zinc chromate [2,3].The precursor of cation exchange modified siliceous material was the synthetic calcium-exchanged silica (SHIELDEX®) which protected steel due to its high pH, through the formation of a siliceous layer and the exchanged of calcium by incoming aggressive ions [4,5]. Other cation exchangers employed as "carriers" are zeolites [6–8]. Zeolites are aluminosilicates that can be exchanged with inhibitive cations [9]. These cations are released in contact with an aggressive aqueous media, and, appropriately chosen, they precipitate in cathodic areas due to the low solubility of their oxides or hydroxides [6,10]. The formation of these insoluble compounds is due to the production of OH^- on the metal surface as a result of the O_2 reduction reaction in cathodic areas [11]. Among the cations exchanged are rare earths ions, that are claimed to inhibit corrosion of zinc, aluminum and steel by forming a passive layer [11–13]. Lanthanides- or rare earths-based compounds were studied as corrosion inhibitors as an alternative to the toxic chromate-based compounds [14–16]. Lanthanides were used as cathodic inhibitors as they formed insoluble hydroxides on the metal substrates [10,14–16]. In addition, they have low toxicity, and their ingestion or inhalation has not been considered harmful to health; the effects of the oxides are similar to those produced for sodium chloride. On the other hand, rare earths are economically competitive given that are relatively abundant

* Corresponding author at: Facultad de Ingeniería, UNLP, Argentina.
E-mail address: c.deya@cidepint.ing.unlp.edu.ar (C. Deya).
[1] In memoriam.

https://doi.org/10.1016/j.porgcoat.2022.107287
Received 28 June 2022; Received in revised form 16 October 2022; Accepted 21 October 2022
Available online 5 November 2022

Table 1
Labeled of the anticorrosive pigments.

Anticorrosive pigment	Observations
H	Washed halloysite
HC	Washed halloysite loaded with Ce(III)
HL	Washed halloysite loaded with La(III)
HCZ	Washed halloysite loaded with Ce(III), and zinc phosphate
HLZ	Washed halloysite loaded with La(III), and zinc phosphate
PZ	Zinc phosphate

in nature.

Taking into account these results, halloysites loaded with praseodymium ions were studied as corrosion inhibitors on Mg alloy AZ31 [17,18].

Besides, lanthanide-exchanged zeolites were studied as anticorrosive pigments for galvanized steel and SAE 1010 steel [19–22].

Recently, halloysites stand out for their ability to trapactive agents, retain and release them [23–26].Halloysites are aluminosilicate clay minerals ($Al_2Si_2O_5(OH)_4$) available in abundance in many locations around the world. They are low cost and non toxic [25,27],whose common forms are the elongated tube or spheroid [25,28,29]. The tubular structure is due to the roll of thin aluminosilicate layers.Halloysite nanotubes trap molecules within the lumen and in the voids between the aluminosilicate sheets or alternatively, the molecules can be adsorbed onto the external surface of halloysite. Part of the ability to exchange cations is permanent due to isomorphic replacements, for example of silicon for aluminum in the tetrahedral sheet. However, much of it is pH dependent and lies in the Si-O-Al junctions on the lateral edges of the crystals, on which the protonation-deprotonation phenomena occur. Halloysites were also tested as carrier for corrosion inhibitors [8,23,30,31].Halloysites nanotubes loaded with Ce^{3+}/Zr^{4+} were incorporated in silane coatings and tested for corrosion protection for metals such as aluminum alloy A356.0 and magnesium alloy AZ91 [32–34]. Results indicate that the ions are released on demand and self-healing protection occurs on damage or degraded areas of the coating.

Taking into account the good results achieved by the loading of zeolites with rare earths metal, and those with loaded halloysite in sol-gel coatings to protect metals, the aim of this work was to study a natural halloysite as carrier pigment, containing ions Ce(III) or La(III),that incorporated into a paint protects steel from corrosion.

The mineral was studied by Fourier transform infra-red spectroscopy and X-ray spectroscopy and modified by loading the halloysite with Ce (III) or La(III) ions. The cationic loaded was studied by inductively coupled plasma atomic emission spectroscopy (ICP-AES spectroscopy) and gravimetrically, and by kinetics released determinations. Electrochemical tests such as corrosion potential measurements and Tafel polarization curves of steel immersed in the mineral and halloysite loaded suspensions in NaCl 0.05 M solution were also carried out. Besides, alkyd anticorrosive paints containing the loaded halloysites, alone or as additives, with zinc phosphate as main anticorrosive pigment, were formulated. Steel painted panels were exposed in salt spray and in humidity chambers, and corrosion and blistering degrees were evaluated. Electrochemical tests such as corrosion potential measurements and ionic resistance determinations were also carried out on painted metal immersed in NaCl 0.5 M solution.

Results showed that the steel is protected when immersed in loaded halloysite suspensions. Besides, anticorrosive paint containing cerium or lanthanum loaded halloysite and zinc phosphate can be used in non-aggressive media with good results.

2. Materials and methods

2.1. Materials

The halloysite used in this research was extracted from natural deposits located in an area called Buitreraat southwest of the province of Rio Negro, Argentine [29,35,36].Other materials used were NaCl, hydroxyquinoline, nitric acid,NH_4CH_3COO, acetic acid, provided all by Anedra in analytical degree, ethanol (96°, Purocol, Argentina), zinc phosphate (SNCZ), $La(NO)_3{\bullet}6H_2O$ (Merck, analytical degree), $Ce(NO_3)_3{\bullet}6H_2O$ (Aldrich, analytical degree). The paints were prepared employing titanium dioxide (Kronos), barite and talc provided by Camuati, Argentina, white spirit (Disa) and toluene (Dorwil) and an alkyd resin (Alkipol 434–50 A, Diransa, Argentina). The additives Tego 652, TEGO 270 and TEGO 460 were provided by TEGO while the driers Co- and Ca- octoates were provided by Casal de Rey, Argentina.

2.2. Characterization of the mineral

2.2.1. FTIR and XRD spectra

FTIR spectrum of the mineral was carried out by the KBr technique employing a Perkin Elmer Spectrum One Spectrometer. The scanned wavelength range was between 600 and 4000 cm^{-1}.

XRD analysis of the total rock and the clay fraction were performed to characterize the mineralogical composition of the material, as well as to identify the clay minerals. The samples were disaggregated and pulverized in an agate mortar. Clay fractions (<2 μ) were separated from all samples by timed sedimentation and then, three samples were prepared per the glass slide method [37]: a) natural, air-dried at laboratory room temperature sample; b) glycolated, sample exposed to the vapours of an ethylene glycol solution for at least 24 h; c) calcined, sample brought to 550 °C for 2 h. X-ray diffraction patterns were collected using a PAN-analytical, model X'Pert PRO diffractometer with Cu tube (Kα = 1.5403 Å) and operating at 40 mA and 40 kV. Angles of 4 to 37° are scanned for the total rock samples, 2 to 32° for the natural samples of the clay fraction, 2 to 27° for the glycolated samples of the same fraction, and 3 to 15° for the calcined samples, with a scanning speed of 0.04° / s.

2.2.2. Electrochemical determinations

Previously to use the mineral in the electrochemical determinations, it was washed with distilled water twice. From now on, the washed mineral would be labeled as H (Table 1).

Corrosion potential measurements were done employing SAE 1010 steel, previously degreased and sanded up to 1000 with sandpaper, as working electrode. The edges of the electrode were sealed with bee-wax leaving an exposed area of 1 cm^2. This electrode was immersed in suspension of 1 g of H, with NaCl 0.05 M as electrolyte. Saturated calomel electrode (SCE) was used as reference. The measurements were carried out during 4 h.

Tafel curves were also performed employing SAE 1010 as working electrode immersed in 1 g of H suspension and NaCl 0.05 M as electrolyte. SCE was used as reference electrode and a platinum rod as counter-electrode. Polarization curves were obtained employing a Gamry Interface 1000 potentiostat / galvanostat, after 5 and 24 h of immersion, using a potential range of −250 to +150 mV from the open circuit potential at a scanning rate of 1 $mV{\cdot}s^{-1}$.

2.2.3. Steel surface observation

SAE 1010 steel, immersed for 24 h in NaCl 0.05 M and H suspension, was observed by scanning electron microscopy (SEM) and the film formed on it was characterized by energy dispersive X-ray analysis (EDS) employing a FEI Microscope Quanta 200 model and an EDXA with Apollo 40 detector.

2.3. Cation modifications

The mineral was washed twice with distilled water. Ten grams of the mineral was added to 25 mL of 1 M $Ce(NO_3)_3{\bullet}6\ H_2O$+ 10^{-3} M HNO_3in a vacuum jar for 24 h under constant stirring. The acid was employed to avoid the precipitation of cerium hydroxides and nitric acid was specifically chosen to avoid the incorporation of an extra anion in the

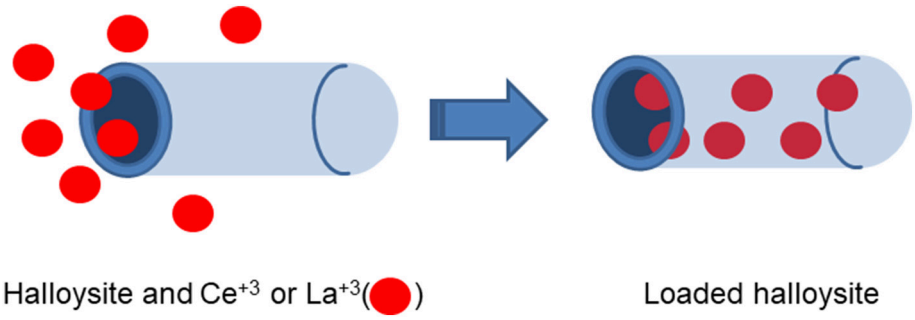

Fig. 1. Loading of the halloysite with the passivating ions.

Table 2
Pigment mixture (% by volume).

Pigment	Pigment mixture					
	pHC	pHL	pHCZ	pHLZ	pZ1	pZ2
HC	10.0	–	2.0	–	–	–
HL	–	10.0	–	2.0	–	–
Zinc phosphate	–	–	10.0	10.0	10.0	30.0
Barite	38.1	38.3	34.1	34.1	35.2	29.2
Titanium dioxide	13.8	13.8	19.6	19.6	19.6	11.6
Talc	38.1	38.1	34.3	34.3	35.2	29.2

solution. Then, the jar was evacuated with a vacuum pump for 1 h in order to eliminate the air in the interior of the halloysite and improve cation trapping. Later, the suspension was stirred at atmospheric pressure for 1 h to promote the adsorption of the cations on the halloysite surface [23]. The cycle vacuum-atmospheric pressure was carried out three times. Finally, the suspension was filtered and the solid was dried at 90 °C until constant weight.

The same procedure was carried out employing 1 M $La(NO)_3$•6 H_2O + 10^{-3} M HNO_3solution in order to obtain the La-loaded halloysite.

Fig. 1 shows a scheme of the halloysite loading.

2.4. Cation loading capacity and release kinetics

The suspensions for analysis were prepared by stirring constantly 1 g of $Ce^{3+}$and La^{3+} loaded H (HC and HL, respectively) in 100 mL of a 1 M NH_4CH_3COO solution, for 24 h at 710 rpm. The supernatant was removed, centrifuged, and analyzed by inductively coupled plasma atomic emission spectroscopy (ICP-AES spectroscopy) and gravimetric technique.

The gravimetric technique was as followed [38]: 10 mL of 2 M acetic acid solution were added to 70 mL of the supernatant and then an excess of 3 % (weight/volume, *w/v*) of 8-hydroxyquinoline (C_9H_7NO) in

Table 3
Density and oil absorption of the pigment mixtures and CPVC, PVC and volume of resin of the paints.

Pigment mixtures		Density (g/mL)	Oil absorption (mL/g)	Paints	CPVC	PVC	Volume of resin (mL/ 100 mL of pigment mixture)
10 % HC	pHC	3.4	0.21	PHC	0.59	0.41	143.9
10 % HL	pHL	3.4	0.21	PHL	0.59	0.41	143.9
2 % of HC + 10 % PZ	pHCZ	3.90	0.14	PHCZ	0.65	0.45	120.5
2 % of HL + 10 % PZ	pHLZ	3.90	0.14	PHLZ	0.65	0.45	120.5
10 % PZ	pZ1	3.60	0.19	PZ1	0.58	0.40	147.9
30 % PZ	pZ2	3.53	0.23	PZ2	0.55	0.38	159.8

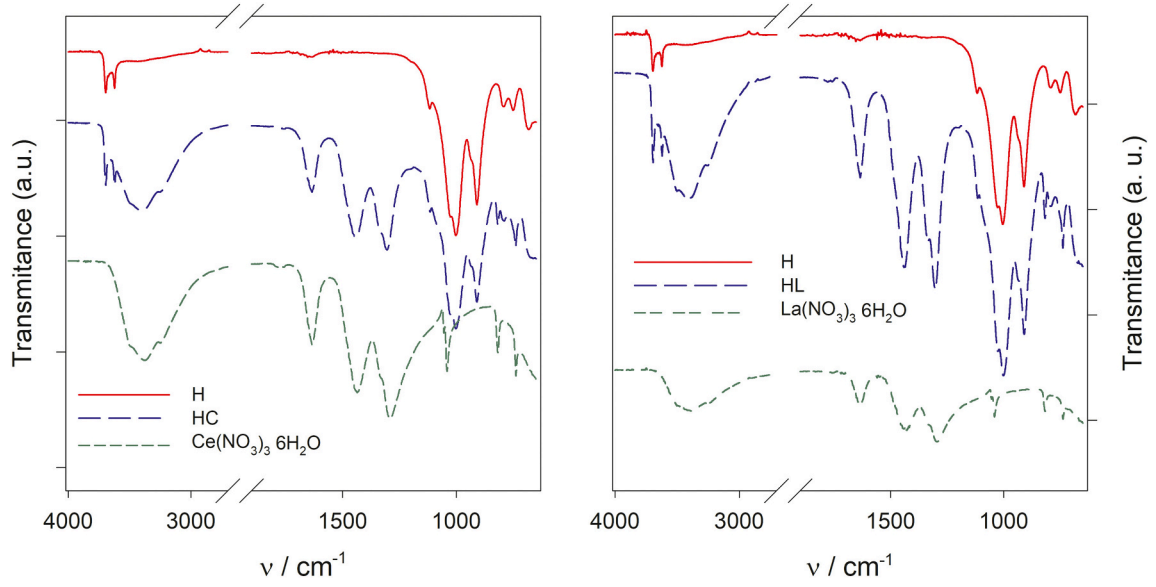

Fig. 2. FTIR spectra of a) halloysite (H), Ce-loaded halloysite (HC) and $Ce(NO)_3$•6 H_2O; b) halloysite (H), La-loaded halloysite (HL) and $La(NO)_3$•6 H_2O.

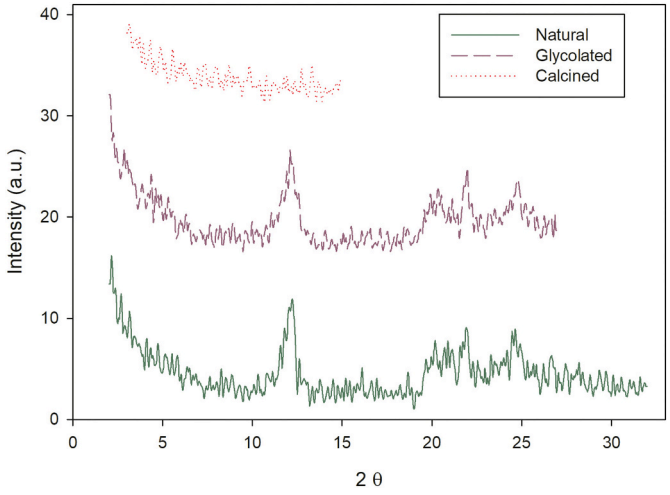

Fig. 3. X-ray spectra of the mineral used.

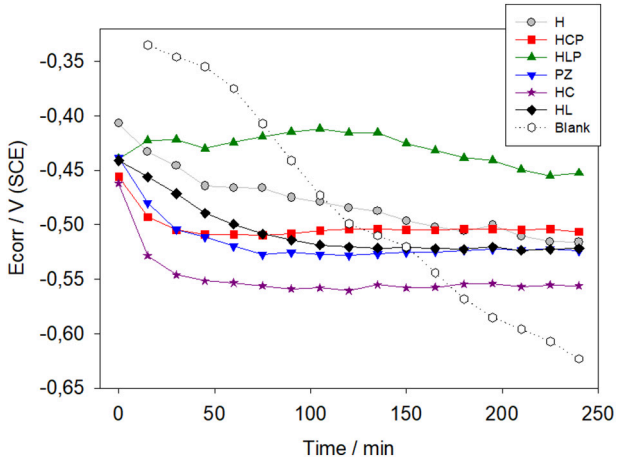

Fig. 4. Corrosion potential of SAE 1010 steel immersed for 4 h in different suspensions in NaCl 0.05 M.

ethanol was added. The excess of 8-hydroxyquinoline is noticed by an orange colour in the solution. Then, 20 mL of 10 % w/v of NH_4OH were added and the solution heated until boiling. The precipitate was separated from the flask by centrifugation at 2200 xg for 5 min. Afterwards it was washed with hot water, dried in a stove at 110 °C and weighed in an analytical scale.

The control samples were prepared employing 70 mL of $Ce(NO_3)_3$ or $La(NO_3)_3$ 0.14 % *w/v* of Ce(III) or La(III), respectively. In every case, determinations were done by triplicate.

The release kinetics was investigated in NaCl solution at room temperature. Loaded halloysites (1 g) were suspended in 50 mL of a 1 M NaCl solution, for 24 h and stirred at 710 rpm, with a magnetic stirrer, in order to establish equilibrium condition and to increase the release rate. Samples for analysis were taken at 1, 2, 4, 6, and 24 h. The cerium and lanthanum concentrations were determined by ICP-AES spectroscopy.

2.5. Loaded halloysites characterization

2.5.1. FTIR spectra

The infrared spectra of the halloysite loaded with $Ce(NO)_3$•6 H_2O (HC) or $La(NO)_3$•6 H_2O (HL), as KBr pellets, were obtained by a FTIR spectrometer (Spectrum, Perkin Elmer, USA) according to diamond ATR method, in order to identify their chemical structure. The FTIR spectra were recorded in the 4000 to 600 cm^{-1} range and scanned with background correction at 60 scans with 4 cm^{-1} resolution.

2.5.2. Electrochemical determinations

Corrosion potential measurements were done during 240 min immersing SAE 1010 electrodes in suspensions of HC and HL with NaCl 0.05 M as electrolyte. A saturated calomel electrode was used as reference.

Tafel fitting was carried out for the potentiodynamic polarization data obtained using SAE 1010 as working electrode immersed in HC or HL suspensions and NaCl 0.5 M as electrolyte after 5 and 24 h. The reference electrode was the SCE and a platinum rod was used as counter-electrode. The potential scan range, from the open circuit potential, was −250 to +150 mV (due the anodic current reached values higher than 10^{-2} A.cm^{-2}at this overpotential) and a scan rate of 1 mV·s^{-1}.

Moreover, Ecorr and polarization curves, Tafel mode, were also done on similar cells but employing the loaded halloysites + zinc phosphate mixtures (1 g + 1 g, respectively); zinc phosphate suspension and the electrolyte without anticorrosive pigment (Blank) were used as controls.

The electrochemical determinations were performed in duplicates

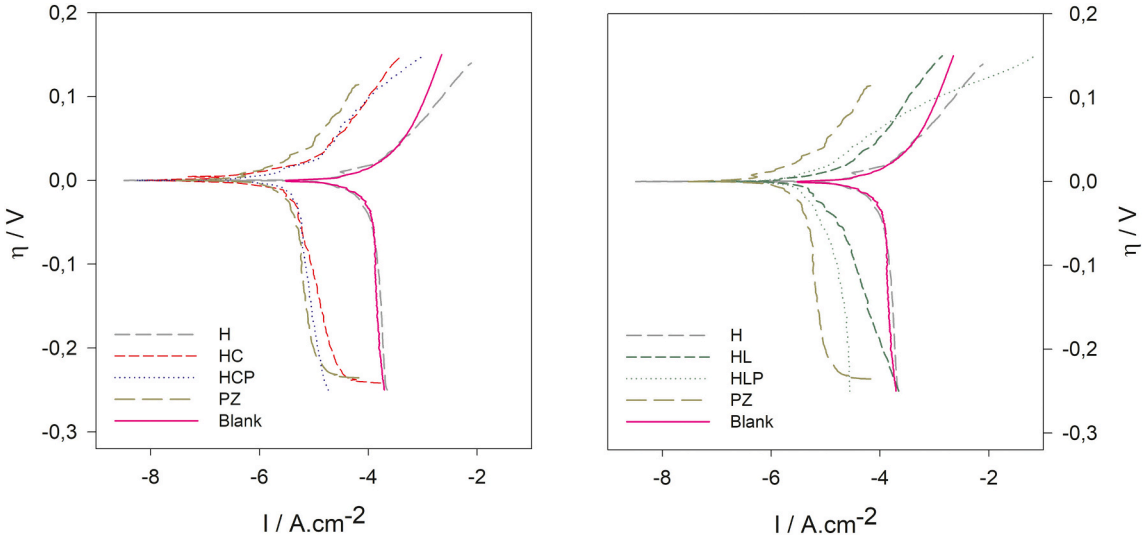

Fig. 5. Polarization curves, Tafel mode, of SAE 1010 steel after 5 h of immersion in 0.5 M NaCl and a) Ce- loaded halloysite b) La-loaded halloysite.

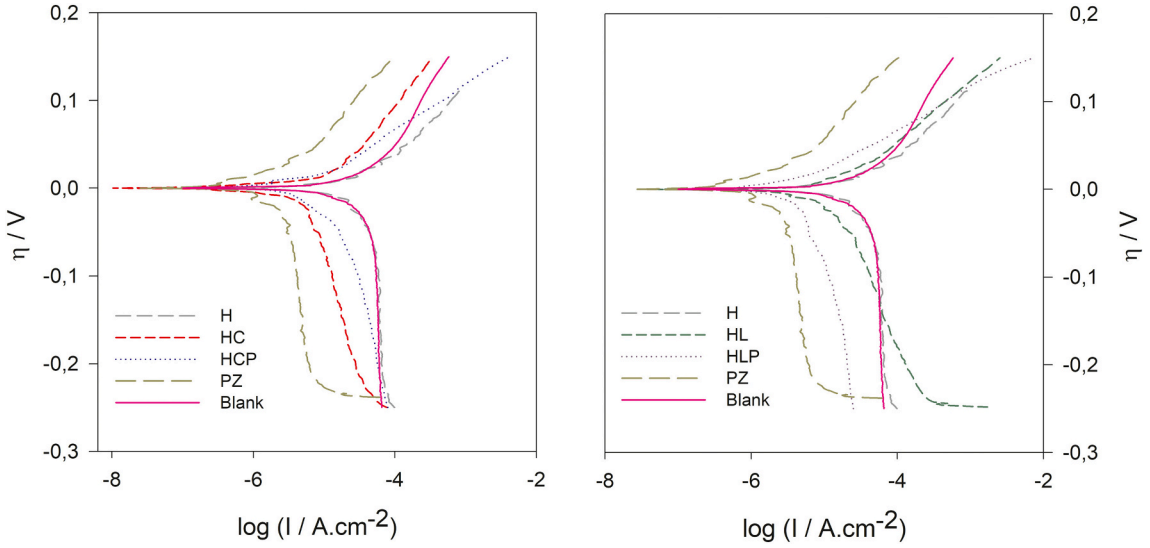

Fig. 6. Polarization curves, Tafel mode, of SAE 1010 steel after 24 h of immersion in 0.5 M NaCl and a) Ce- loaded halloysite b) La-loaded halloysite.

Table 4
Corrosion potential (Ecorr), corrosion current (Ic) and inhibition efficiency for SAE 1010 steel immersed in the suspensions after 5 and 24 h.

Suspension	Ecorr (V vs SCE)		Ic (μA.cm^{-2})		Inhibition efficiency (%)	
	5 h	24 h	5 h	24 h	5 h	24 h
H	−0.581	−0.603	124.1	52.8	No inhibition	40.6
HC	−0.576	−0.596	2.7	4.5	96.5	94.9
HL	−0.578	−0.581	10.4	9.5	86.4	89.3
HCP	−0.542	−0.547	3.7	17.6	95.3	80.2
HLP	−0.492	−0.500	10.6	8.2	86.5	90.8
PZ	−0.602	−0.566	3.2	3.8	95.9	95.7
Blank	−0.629	−0.602	78.8	89.0	–	–

and employing a Gamry Interface 1000 potenciostat / galvanostat. Details of these tests were given in Section 2.2.

The labels of the anticorrosive pigments used can be seen in Table 1.

2.5.3. *Surface characterization*

After 24 h of immersion in NaCl 0.05 M and HC, HL, HCP, HLP or

Table 5
Loading capacity of cerium and lanthanum ions determined by different techniques.

	mg Ce/g		mg La/g	
	ICP/NH_4^+	Gravimetry	ICP/NH_4^+	Gravimetry
Halloysite	147.4	180	156.8	137

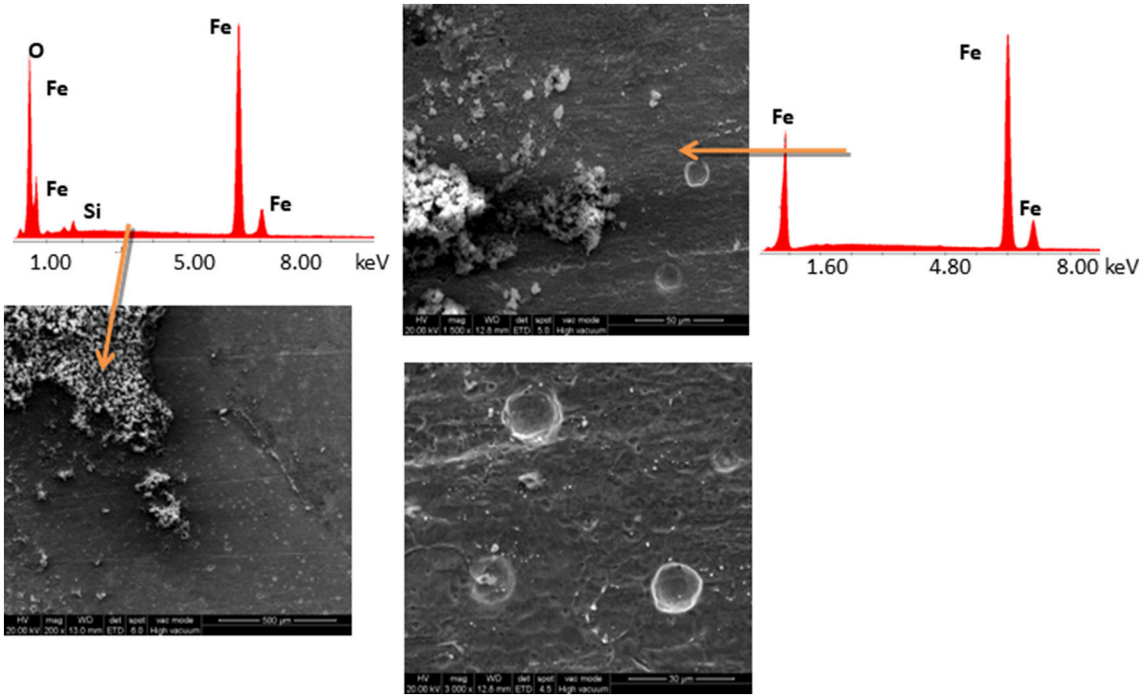

Fig. 7. SEM micrographs and EDX of the steel substrate immersed in the halloysite suspension for 24 h.

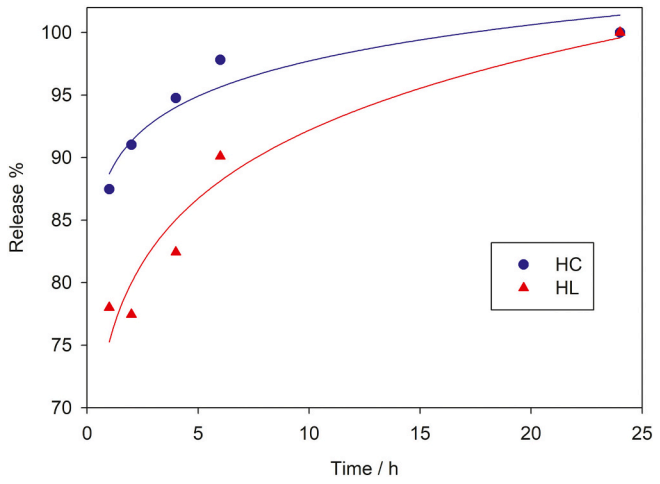

Fig. 8. Release (%) of the cations from the loaded halloysites. Dots: experimental data; lines: fitting curves.

zinc phosphate (PZ) suspensions the surface of SAE 1010 was observed by SEM and characterized by EDXA, in the same equipment as H. High vacuum mode was used and micrographs at 200, 1500 and 3000 X were taken.

2.6. Paint formulation, preparation and application

In order to formulate the anticorrosive paints with the loaded halloysites, the density of the halloysite was obtained by the pycnometric method according to ASTM G 1475.

The pigment mixtures were obtained mixing 10 % by volume of the loaded halloysites HC and HL (pHC and pHL, respectively) with barite, titanium dioxide and talc (Table 2). Besides, pigment mixtures with 2 % of HC or HL and 10 % of zinc phosphate (pHCZ and pHLZ, respectively), 10 % of zinc phosphate (pZ1) and 30 % of zinc phosphate (pZ2) were also prepared.

The density and the oil absorption (ASTM D281)of the pigment mixtures were determined in order to calculate the CPVC (critical pigment volume concentration). Tests were done in triplicates.

CPVC was calculated as:

$$CPVC = \frac{1}{1 + \frac{Oil\ volume}{weight\ pigment\ mixture} \times \delta pigment\ mixture} \quad (1)$$

being *Oil volume* and *weight pigment mixture*, the volume of linseed oil and the mass of pigment mixture, respectively, used in the oil absorption determinations and δ*pigment mixture* the density of the pigment mixture determined by the pycnometric method.

The PVC was calculated as.

$$PVC = 0.7 \text{ x } CPVC \quad (2)$$

being PVC the pigment volume concentration (Table 3).

The formulations were done in order to study the possible replacement of part of zinc phosphate by the loaded halloysites. Alkipol 434–50 A, an alkyd resin based on soya oil (50 % of solids in white spirit) was used as film forming material while white spirit was used as solvent. TEGO 652 was added as wetting and dispersing additive.

Paints were prepared in a ball mill, adding all the components together and milled for 24 h. Just before painting, TEGO 270 and TEGO 460, 0.45 % *w*/w each from the total paint formulation, were added as wetting and leveling agents, respectively. Besides, Co- and Ca- octoates were added as driers (0.1 % and 0.5 % w/w, respectively).

SAE 1010 steel panels were sandblasted until a Sa 2 ½ degree (SIS 05 59 00) and degreased with toluene. Afterwards, the panels were painted by brush until a 70 ± 15 μm dry thicknesses, measured employing a Schwyz SC117–02 Coating Thickness Gauge.

Panels were left under laboratory conditions for 7 days before testing.

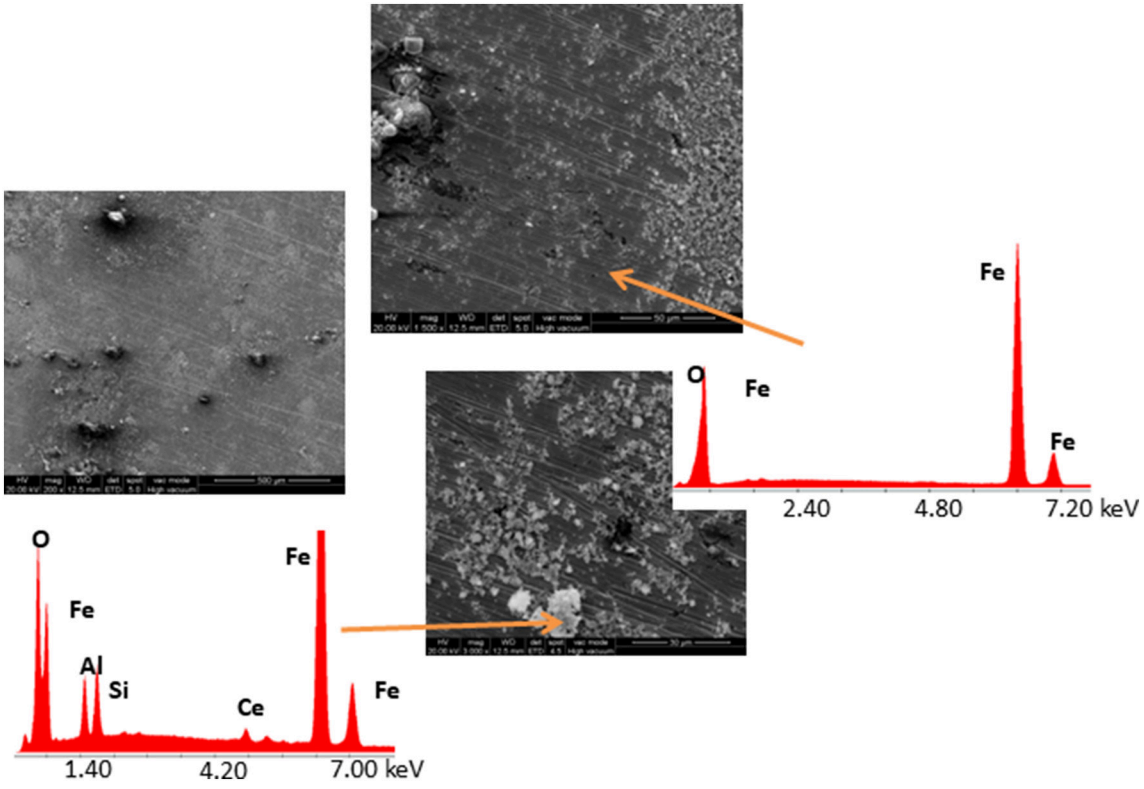

Fig. 9. SEM and EDS spectrum of steel immersed 24 h in HC suspensionin NaCl 0.05 M.

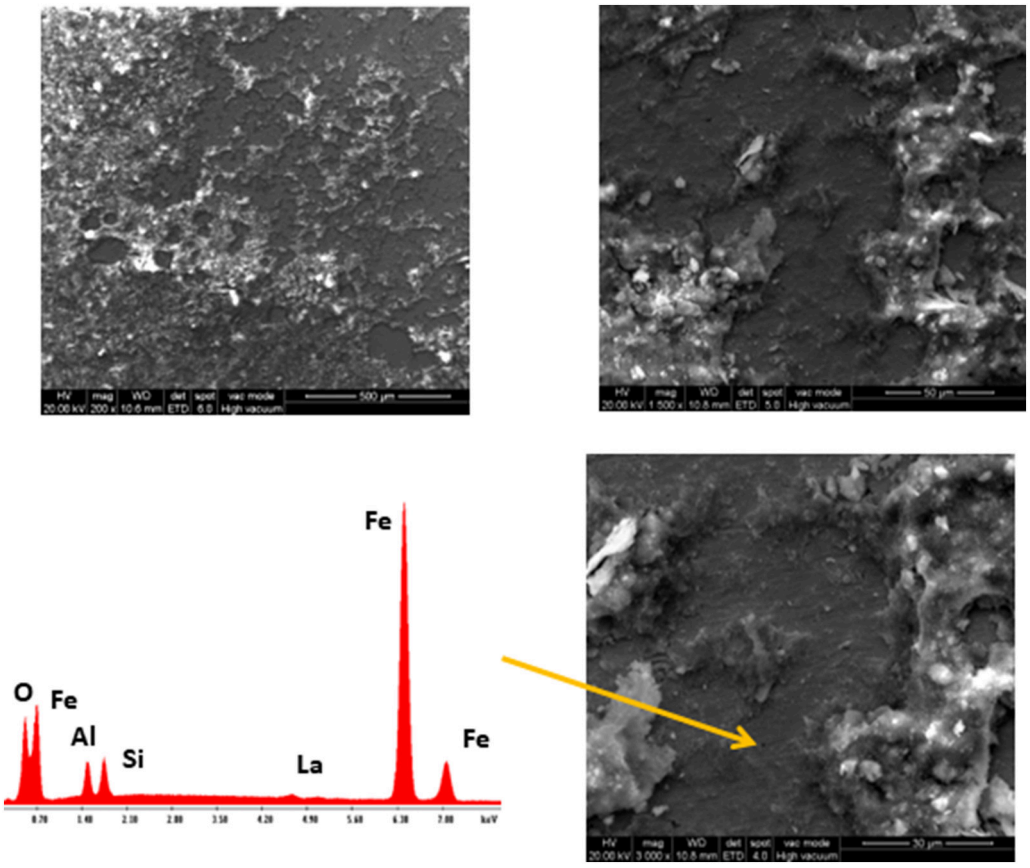

Fig. 10. SEM and EDS spectrum of steel immersed 24 h in HL suspension in NaCl 0.05 M.

2.7. Tests on the painted panels

2.7.1. Accelerated tests

Painted panels were place in the salt spray (ASTM B117) and humidity (ASTM D2247) chambers and corrosion (ASTM D 610) and blistering (ASTM D 714) degrees were evaluated during 936 and 504 h, respectively.

2.7.2. Electrochemical tests

Electrochemical tests were done on cells prepared attaching, on the painted panels, a cylinder with epoxy glue. The cylinders were filled with 12.5 mL of 0.5 M NaCl and corrosion potential and ionic resistance were determined during 28 days. In the first case, a saturated calomel electrode (SCE) was used as reference and in the second, a platinum ring was employed. The corrosion potentials were measured employing the Gamry Interface 1000 potenciostat / galvanostat and the ionic resistance employing an ATI Orion Model 170 conductivity meter at 1000 Hz.

3. Results and discussion

3.1. Characterization of the mineral

3.1.1. FTIR analysis

FTIR spectrum of the halloysite mineral (H) shows bands at 3696 cm^{-1} and 3622 cm^{-1} attributed to the stretching vibration modes of symmetric in-phase inner surface hydroxyl and inner hydroxyl, respectively. A band at 910 cm^{-1} associated with the bending vibration of inner surface hydroxyl and bands at 1025and 792 cm^{-1} due to Si—O bond can be seen [39,40]. No band appeared at 3550 cm^{-1} indicating the absence of interlayer water (Fig. 2).

3.1.2. X-ray analysis

The x-ray spectrum of the mineral shows a peak at $2\theta = 12°$, related to a basal spacing layers of 7 Å, characteristic of dehydrated halloysite [41,42], confirming the data from FTIR spectrum. Besides, the peaks that appeared at 20.2° and 24.5°, correspond to 4.44 and 3.58 Å spacing, representative of 1:1 type of clays [41] (Fig. 3). According to the JCPDS, the halloysite file number is 29–1487.

The characteristic basal reflections show that the interlayer distances of glycolate modified clay sample remained unchanged, indicating that expansion of ethylene glycol into the interlayer of halloysite did not occur. Furthermore, the diffractogram of the calcined sample shows that the heat treatment produces a collapse of the crystalline structure of the mineral, causing the disappearance of the reflection at 7 Å.These results indicate that most of the interlayer inner-surface AlOH groups of halloysite were unavailable, since they were blocked by the strong hydrogen bonds between layers [27].

3.2. Electrochemical determinations

3.2.1. Corrosion potential measurements

The corrosion potential (Ecorr) of steel immersed in the halloysite suspension (Fig. 4) diminished continuously being, during the first days of assay, more negative than the blank, indicating an attack on the steel surface. However, after 105 min, the values were more positive probable due the deposits of halloysite on the metal surface that block reactive sites.

3.2.2. Polarization curves, Tafel mode

The anodic and cathodic currents in the polarization curves, Tafel mode, were similar to the blank, indicating that the mineral does not affect the behaviour of the metal in NaCl solution (Fig. 5).The same behaviour was obtained after 24 h of immersion (Fig. 6). The values of

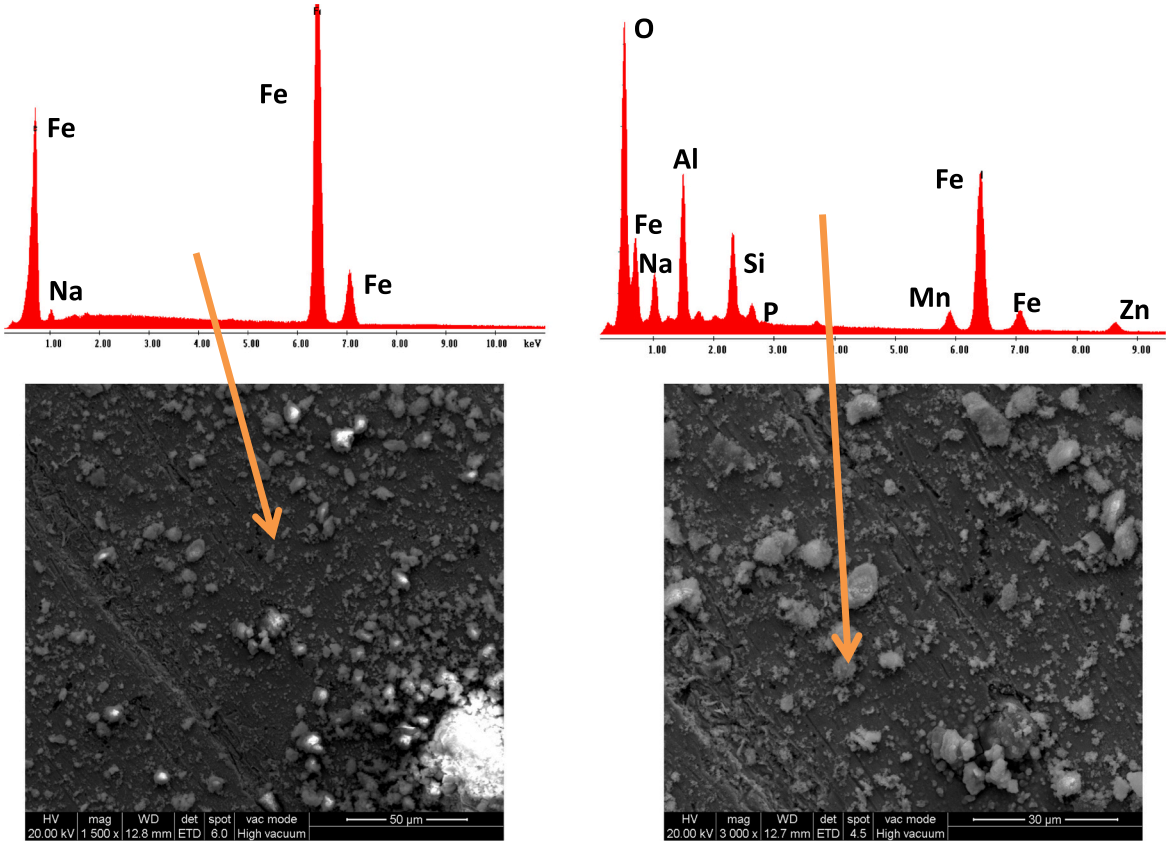

Fig. 11. SEM and EDS spectrum of steel immersed 24 h in HCP suspension in NaCl 0.05 M.

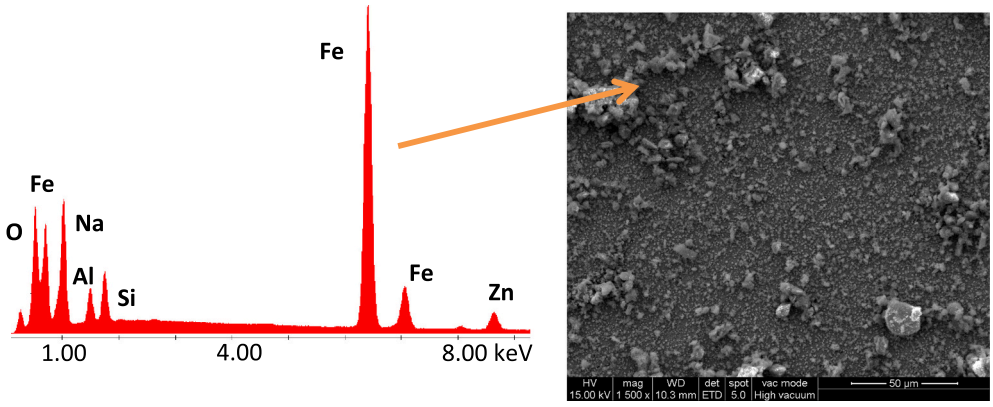

Fig. 12. SEM and EDS spectrum of steel immersed 24 h in HLP suspension in NaCl 0.05 M.

the corrosion current were of the same order of magnitude and the inhibitory efficiency (IE), calculated according to the following Eq. (3):

$$IE(\%) = 100 \bullet (I0 - I)/I0 \quad (3)$$

showed there is no inhibition after 5 h of immersion and that it is not significant after 24 h (Table 4). The differences in Icorr may be due to the deposit of H on the metal surface that is not enough to prevent corrosion.

3.2.3. *Surface characterization*

A homogenous layer containing Fe, with round cavities of 15 µm diameter was observed by EDS on the steel surface immersed in the halloysite suspension. Besides, some halloysites seemed to be deposited on the surface as structures containing Si and O are present. These deposits may be blocking some actives sites while the round cavities are signs of localized corrosion (Fig. 7).

3.3. *Cation loading capacity and release kinetics*

The loading capacity of the halloysite for cerium and lanthanum ions, determined by ICP and gravimetrically, is of the same order of magnitude and there are no differences in the Ce and La loaded due to the similar radii and charge of the ions (Table 5).

The weight of Ce(III) and La(III) determined from the gravimetrical method was calculated from the molecular formula of the precipitates obtained.

The purple-brown precipitate $Ce(C_9H_6ON)_4 \bullet 2H_2O$ has a molecular weight of 752.2 and an amount of Ce of 140.2, then, the amount of Ce

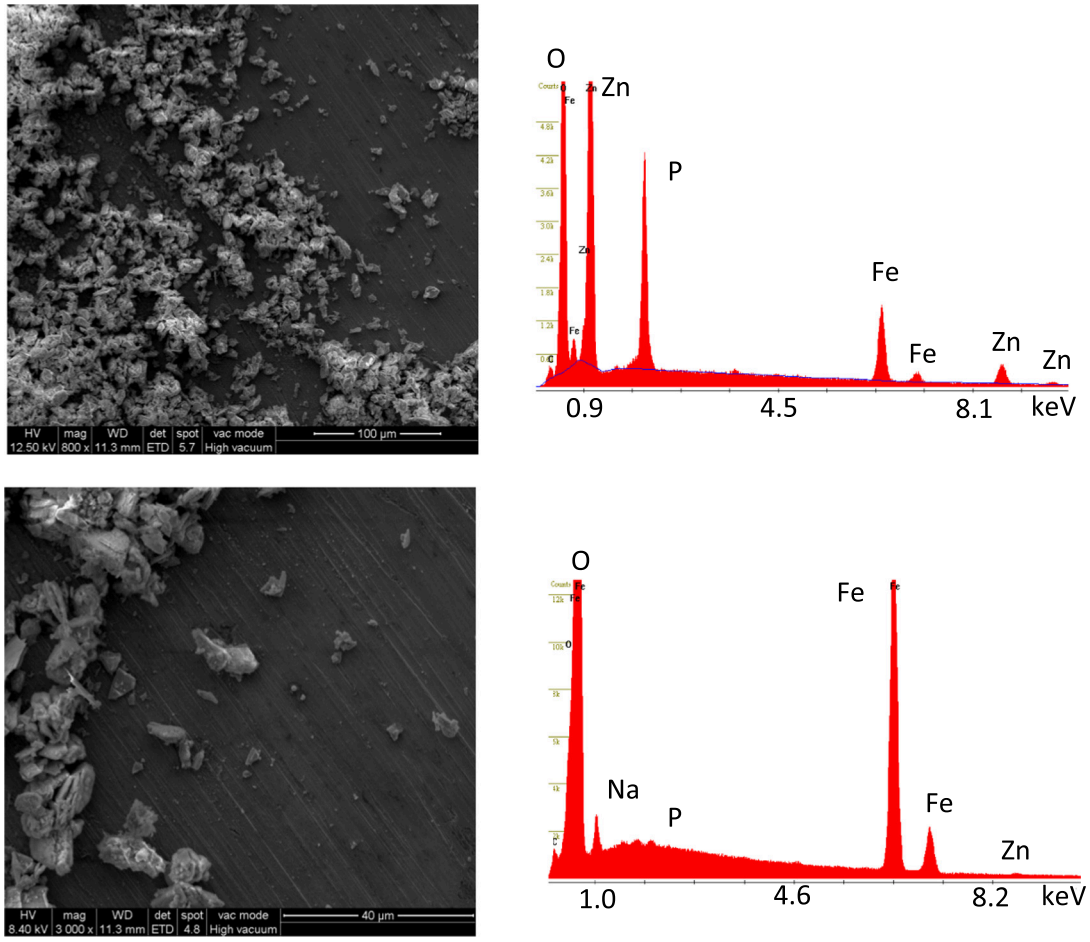

Fig. 13. SEM and EDS spectrum of steel immersed 24 h in PZ suspension inNaCl 0.05 M.

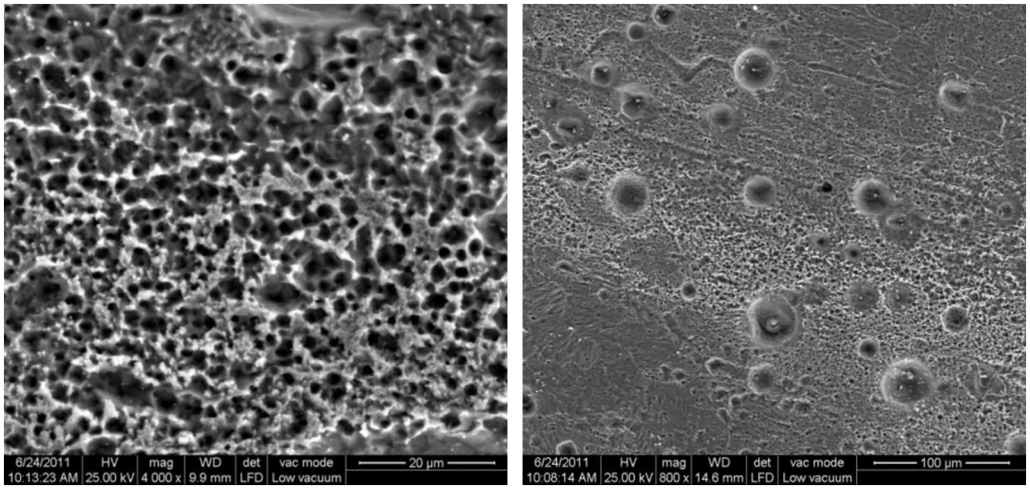

Fig. 14. SEM of steel immersed 24 h in NaCl 0.05 M.

per g of precipitate was calculated as

$$\frac{mg\ Wc}{g\ precipitate} = \frac{Wc \times 140.2}{752.2} \times 1000 = 186 \times Wc \quad (3)$$

being Wc the weight of the precipitate obtained.

In the case of La, the yellow precipitate has the formula La $(C_9H_6ON)_3 \bullet 2H_2O$, being its molecular weight 570.9 and 138.9the-amount of lanthanum. In this case, being Wl the weight of the precipitate obtained,

$$\frac{mg\ Wl}{g\ precipitate} = \frac{Wc \times 138.9}{570.9} \times 1000 = 243 \times Wl \quad (4)$$

is the amount of La per g of precipitate.

The kinetic released was followed by ICP determinations for cerium and lanthanum ions (Fig. 8).Cerium ions are released more rapidly than lanthanum ions but both of them are released almost immediately;

Table 6
Corrosion (ASTM D 610) degree of the painted panels exposed in the salt spray chamber (ASTM B117).

Paint	Time (hours)			
	360		672	
	R	B	R	B
PHC	–	–	–	–
PHL	–	–	–	–
PHCZ	10	10	7	2 MD
PHLZ	10	10		
PZ1	10	10	Important degradation	
PZ2	10	10	10	10

almost 100 % of the ion was released after 24 h of immersion.

The profile rate of release of inhibitors indicated that in the initially phase there are ions loss by diffusion from the outer surface of the halloysite, known as the burst effect [43]. This phenomenon leads to higher initial active substance delivery and reduces the durability of the protection.

The results show that the protection afforded by the loaded halloysites might occur during a short period. These would suggest that these loaded halloysites might be used together with other anticorrosive pigments in order to lengthen the protection or coated with a suitable polymer as a strategy to reduce inhibitor rate release, according to recent advances reviewed by Lvov et al. [44,45] about of halloysites-polymer nanocomposites toward controlled release.

3.4. Characterization of the loaded halloysites

3.4.1. FTIR spectra

The FTIR spectra of HC and HL together with those of $Ce(NO_3)_3$, $La(NO_3)_3$, are showed in Fig. 2a) and b).The salts presented bands at 3400 and 1645 cm^{-1} due to stretching and bending vibrations of water and at 1444, 1291, 1040, 816 and 738 cm^{-1} due to nitrate ions vibrations. The loaded halloysites presented bands due to the mineral and to the salts, indicating that the load was successful and that no important modifications occurred on halloysite structure.

3.4.2. Electrochemical determinations

In general, Ecorr values (Fig. 4) diminished constantly over time for 70 min and then the values were almost constant until the end of the assay. After 240 min, Ecorr values of steel immersed in H, HL, HCP and PZ suspensions were around −0.52 V and of those immersed in HC suspension around −0.55 V. In the case of panels immersed in HLP suspension, Ecorr increased slightly for 100 min, and then it diminished reaching −0.45 V after 240 min. In the case of the blank (NaCl solution without inhibitor), Ecorr values diminished continuously from −0.3 to −0.62 V, without reaching a constant value. At the end of the test, the

Table 7
Rusting (ASTM D 610) and blistering (ASTM D 714) degrees of the painted panels exposed in the humidity chamber (ASTM D2247).

Paints	Time (hours)							
	168		408		504		670	
	Ra	Bb	Ra	Bb	Ra	Bb	Ra	Bb
PHC	–	–	–	–	–	–	–	–
PHL	–	–	–	–	–	–	–	–
PHCZ	10	4 M	9P	2 M	–	–	–	–
PHLZ	10	10	7P	10	7P	6F	7P	6F
PZ1	10	2 M	10	2 M	10	2 M	6P	2 M
PZ2	10	10	10	10	10	10	10	10

[a]Rusting degree	10	9	8	7	6	5
Rustedarea / %	< 0.01	0.01–0.03	0.03–0.1	0.1–0.3	0.3–1	1–3

S: spot rusting – the bulk of rusting is concentrated in a few localizes areas. G: general rusting – various size spots are randomly distributed across the surface.

[b]Blisteringdegree				
Frequency	Dense, D	Medium dense, MD	Medium, M	Few, F
Size	10	8	6, 4	2
Comments	No blistering	Smaller size blister easily seen by unaided eye	Progressivelylargersizes	

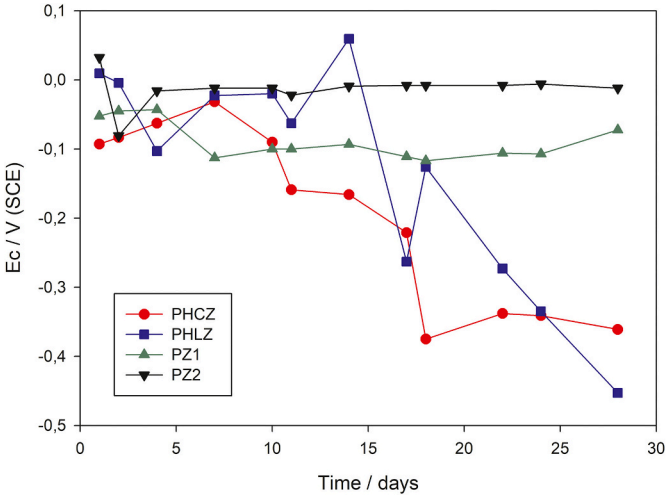

Fig. 16. Corrosion potential (Ec) of the painted panels.

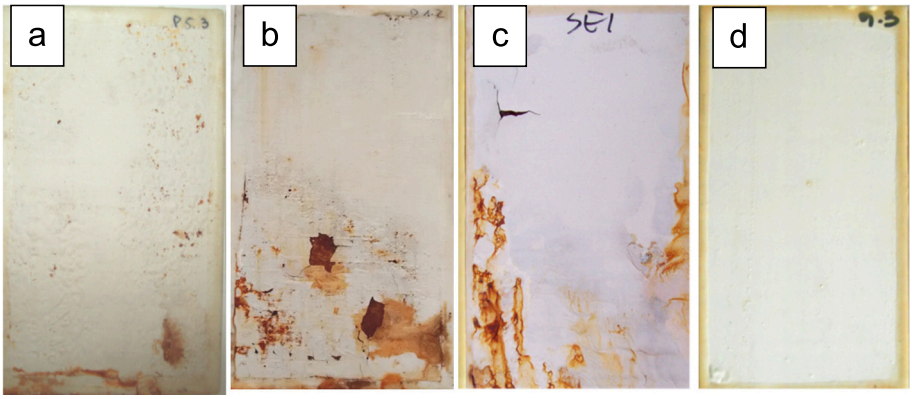

Fig. 15. Panels exposed in the salt spray chamber (ASTM B117) for 672 h; a) PHCZ; b) PHLZ; c) PZ1; d) PZ2.

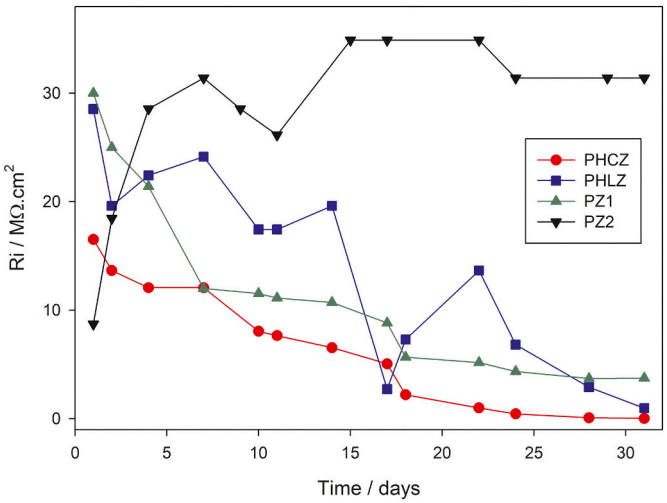

Fig. 17. Ionic resistance (Ri) of the painted panels.

presence of the halloysite and/or zinc phosphate depleted the corrosion potential of steel at least 100 mV toward more positive values, compared to the blank.

Measurements done after 5 and 24 h of immersion (Table 4) showed that Ecorr valuescontinued diminishing, reaching values near the blank (~ −0.6 V) after 24 h. These results indicate that the presence of the inhibitors diminishes steel activity for a short period. Besides, it can be seen that the presence of the passivating ions does not change the behaviour of steel immersed in the halloysite suspensions and that it is similar when zinc phosphate is present.

Tafel curves of SAE 1010 immersed 5 and 24 h in the loaded halloysites suspensions, indicate that the presence of loaded halloysite, without (HC or HL) or with zinc phosphate (HCP and HLP) inhibits the corrosion of the metal (Figs. 5 and 6, respectively). The presence of the halloysite loaded with cerium ions, diminished anodic and cathodic currents to values similar of that in the presence of phosphate, indicating that there is not an adding protection when both inhibitors are used together. In the case of HL, the decreased in the currents was smaller, even when HLP was used showing, in this last case, an interference in the protective behaviour of the inhibitors. These interference could be due to the precipitation of $LaPO_4$,insoluble in water [46] that removes both inhibitors from the solution and the amount of them in the solution is not enough to prevent corrosion. In the case of cerium, $CePO_4$, is also insoluble, but the amount of ions that remain in solution seemed to be enough to protect steel.

The percentages of inhibition efficiency (IE) calculated using Eq. 1 were higher than 85 % after 5 h of immersion, reaching in the case of HC 96.5 %, higher than when PZ was used (95.9 %). After 24 h, only HCP has IE lower than 85 % (Table 4).

The electrochemical tests showed that although the activity of steel immersed in the different suspension is similar, the corrosion rate is much lower when an inhibitive compound was added.

3.4.3. Surface characterization

A thin film containing Fe and O, probably iron oxide, was formed on steel surface immersed in HC suspension (Fig. 9).This is a thin film, as the lines of the sandpapered can easily be seen. On this film, isolated agglomerations containing Si, Al and Ce appeared. In the case of steel immersed in HL suspension, two layers can be seen: a uniform thin film containing La and on top, a discontinuous film formed by agglomerations, probable halloysite as it has Si, Al and La (Fig. 10).

The presence of Ce or La on the metal surface is an indication of the released of the cations from the halloysite.

Steel immersed 24 h in HCP and HLP suspensions (Figs. 11 and 12, respectively) presented a homogenous layer and agglomerations that contain Si and Al (due to the halloysite), Zn and P (due to zinc phosphate). No Ce or La were detected by EDS.

Steel immersed in PZ suspension presented a thin layer (as the lines of the sandpapered can be seen) with low O content and agglomerations on it with higher O content, probably due to the presence of iron oxides (Fig. 13). Zn and P were also present.

In the case of the blank, an important number of cavities were seen on steel surface (Fig. 14). These cavities are due to localized corrosion and were also present on the steel surface immersed in the halloysite suspension but not when loaded halloysites and/or zinc phosphate were incorporated.

3.5. Tests on the painted panels

3.5.1. Accelerated tests

The panels with loaded halloysites paints PHC and PHL were removed from the salt spray chamber after 192 h of exposure, due to the important corrosion degree (qualification 5P: 1–3 % of the surface with corrosion spots). This was probably due to the rapid released of the rare earth cations, that produced the lixiviation of the inhibitive cations from the paint and the loss of the inhibitive action of the loaded halloysite. The rapid released was observed in the kinetic released assay (Section 3.3), almost all the cations were loss after 24 h of immersion.

Panels PHCZ, PHLZ, PZ1 and PZ2 were evaluated with 10 after 360 h of exposure but afterwards, the degradation was important, being PHLZ and PZ1 the ones more degraded (Table 6). The degradation is related to the low amount of anticorrosive pigment in the case of PZ1 [47] while the presence of lanthanum loaded on the halloysite is not enough to protect steel.

Panels PZ2 were qualified with 10 (nor corrosion nor blisters were present) after 672 h (Fig. 15).

In the humidity chamber (Table 7), panels PHC and PHL were removed before 168 h has elapsed due to the important corrosion degradation. Blisters appeared after 168 h in the cases of PHCZ and PZ1 while corrosion spots appeared after 408 h in the cases of PHCZ and PHLZ. After 670 h, the corrosion degree of panels PHLZ was less than of PZ1, having panels PZ1 bigger and more frequently blisters. Panels PZ2 were qualified with 10.

3.5.2. Electrochemical tests

During the first 10 days of immersion, the corrosion potential values (Ec) of the painted panels were around −0.05 V. Afterwards, differences appeared: panels PZ1 and PZ2 have Ec near −0.1 and 0.0 V, respectively, while those of panels protected with paints containing the loaded halloysite diminished continuously reaching values around −0.4 V after 28 days of immersion (Fig. 16). These results indicate that the presence of loaded halloysite in the paint with low phosphate content (PHCZ and PHLZ) interferes with the protection afforded by zinc phosphate.

The ionic resistance (Ri) of panels PHLZ, PZ1 and PZ2 were higher than 10 $M\Omega.cm^2$ for 17 days (Fig. 17). Afterwards, the value diminished, almost constantly reaching 1 $M\Omega.cm^2$ at the end of the assay. In the case of panels PZ2, with the highest zinc phosphate content, Ri increased and after 28 days it was around 30 $M\Omega.cm^2$. As Ri were higher than 1 $M\Omega.cm^2$, certain barrier properties were present in the coatings.

3.6. Mechanism of protection proposed

Considering cited references and this research work, the following mechanism of protection was proposed.

The paints protect the substrates by two main mechanisms: one is due to the barrier properties of the coating and the other is by the active corrosion inhibition due to the presence of anticorrosive compounds. In the case of the barrier mechanism, coatings isolate the metal from the aggressive media by a physical barrier that delays the entrance of water, oxygen, chloride, and other aggressive ions. When the aggressive compounds reach the metal surface electrochemical reactions occur on the

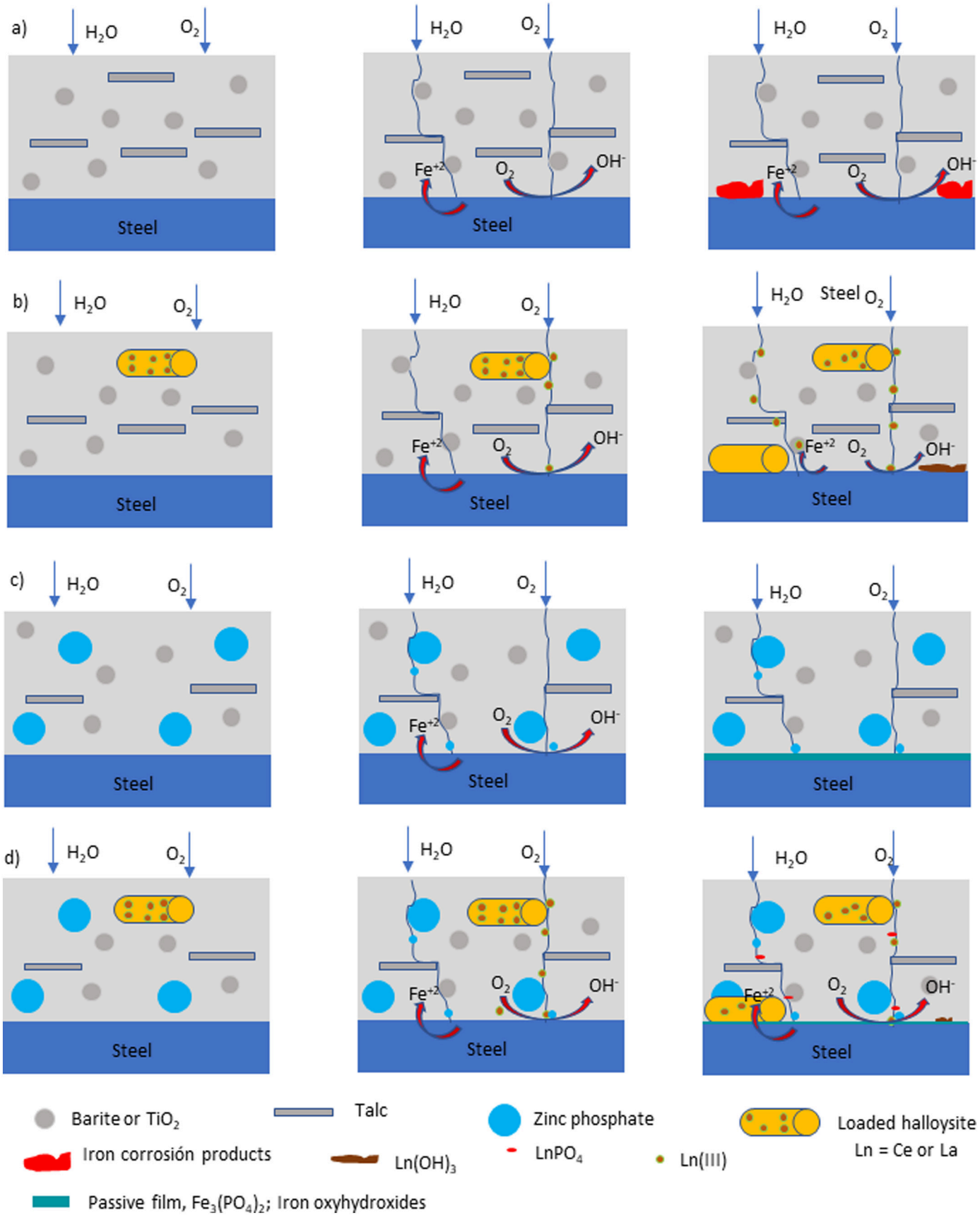

Fig. 18. Scheme of the protection mechanisms.

surface: the metal oxidizes while O_2 is reduced. When the metal is steel, the following reactions occur:

at the anode

$$Fe - - - Fe^{2+} + 2e -$$

at the cathode

$$O_2 + 2H_2O + 4e - - - - - 4\,OH^-$$

If no anticorrosive pigment is present in the paint, corrosion occurs. A scheme of this phenomenon can be seen in Fig. 18a.

If an active corrosion inhibitor is present, it is dissolved by water due to its low solubility, and it goes through the paint together with water and O_2. Corrosion inhibition starts to protect the metal once the barrier properties were loss and the inhibitor reaches the metal surface, which is the place where the corrosion reactions occur. This inhibition can occur by precipitating insoluble compounds on the cathodic area, inhibiting O_2 reduction. In general, this reaction is the precipitation of hydroxides and/or oxides. Ions such as La^{3+} and Ce^{3+}, protect in this way. The corrosion inhibition of lanthanides (Ce and La) is associated with the concentration of cations in the solution. The cations react with the hydroxyl ions of the cathodic oxygen reduction reaction forming highly insoluble hydroxides and oxides according to:

$$Ln^{3+} + 3OH^- - - - - Ln(OH)_3\downarrow$$

$$2Ln(OH)_3 - - - - Ln_2O_3 + 3H_2O$$

being Ln the lanthanide. These compounds precipitate on the metal surface and form a passive layer that inhibits the cathodic current flow resulting in prolonged corrosion resistance.

However, in the cases under study, the leaching speed of the protective ions from the halloysite was very high and when water, O_2, Ce^{3+} and La^{3+} reach the metal surface, most of the passive ions have been washed away and the ones left were not enough to protect steel forming a long-lasting passive oxide film. Some halloysite may be deposited on the steel surface, contributing to certain protection.

A scheme of this phenomenon can be seen in Fig. 18b.

Other type of reaction is the formation of insoluble compounds with the metal ions, such as metal oxides, formed in the anodic area. Is the case of phosphate used to inhibit steel corrosion. Iron phosphate can precipitate on anodic areas or phosphate can enhance the protective properties of the iron oxyhydroxide film formed on the metal surface. A protective film is formed (Fig. 18c).

When zinc phosphate is added to the loaded halloysite, better results were obtained due to the protective action of phosphate ions. However, the precipitation of $CePO_4$ and $LaPO_4$ occurred, far from the metal, as water dissolves the slightly soluble zinc phosphate, and the anion reacts with Ce^{3+} or La^{3+} leached from the halloysite in the paint film.

$$ZnPO_4 - - - - Zn^{2+} + PO_4^{3-}$$

$$PO_4^{3-} + Ce^{3+} - - - - CePO_4\downarrow$$

$$PO_4^{3-} + La^{3+} - - - - LaPO_4\downarrow$$

The precipitation of these phosphates diminishes the amount of inhibitors that reach the metal surface and less active protection is given by the paints (Fig. 18d).

As the protection afforded by the tested paints involves several mechanism and simultaneous reactions further work should be done to confirm this mechanism and give more details.

4. Conclusions

- Halloysites can be loaded with cerium and lanthanum ions and employed to delay steel corrosion in NaCl solutions.
- A homogeneous film partially covered by agglomerations containing Al, Si and the loaded ion is formed on steel immersed in loaded halloysites suspensions in NaCl solution. This film protects steel from corrosion.
- Incorporated in alkyd paints, halloysite loaded with cerium ions can partially replace zinc phosphate, in chloride containing environment. In high humid environment, halloysite loaded with lanthanum can partially replace zinc phosphate.
- Good agreement between accelerated and electrochemical tests was obtained.
- Besides, considering the inhibition afforded by the loaded halloysites of steel corrosion in solution, the high release rate of the ions and the lower performance in alkyd paints, it is worthwhile to study the possibility of encapsulated the loaded halloysite in order to control ionic release rate.

CRediT authorship contribution statement

S. Roselli: Investigation, Methodology, Writing – original draft. **M. Revuelta:** Investigation, Methodology, Writing – original draft. **C. Deya:** Conceptualization, Writing – review & editing, Resources, Visualization, Supervision.

Declaration of competing interest

The authors declare that they have no known competing financial interests or personal relationships that could have appeared to influence the work reported in this paper.

Data availability

Data will be made available on request.

Acknowledgments

The authors wish to thank the CONICET (Consejo Nacional de Investigaciones Científicas y Técnicas), CICPBA (Comisión de Investigaciones de la Provincia de Buenos Aires) and Universidad Nacional de La Plata for their financial support to do this research.

We are grateful to Lic. Alexis Martinez and Lic. Fernando Pestalardo, owners of BIOTEC S.A., the company that exploits the deposits, for providing us with the Halloysite.

References

[1] M.N. Khan, F. Mohammad, Eutrophications: challenges and solutions, in: A.A. G. Ansari, Savajeet Singh (Eds.), Eutrophication: causes, consequences and control, vol 2, Springer, 2014, pp. 1–16.
[2] B. Chico, J. Simancas, J.M. Vega, N. Granizo, I. Diaz, D. de la Fuente, M. Morcillo, Anticorrosive behaviour of alkyd paints formulated with ion-exchange pigments, Progr. Org. Coat. 61 (2008) 283–290.
[3] N. Granizo, J.M. Vega, D. de la Fuente, B. Chico, M. Morcillo, Ion-exchange pigments in primer paints for anticorrosive protection of steel in atmospheric service: anion-exchange pigments, Progr. Org. Coat. 76 (2013) 411–424, https://doi.org/10.1016/j.porgcoat.2012.10.009.
[4] N. Granizo, J.M. Vega, I. Díaz, B. Chico, D. de la Fuente, M. Morcillo, Paint systems formulated with ion-exchange pigments applied on carbon steel: effect of surface preparation, Prog. Org. Coat. 70 (2011) 394–400, https://doi.org/10.1016/j.porgcoat.2010.09.035.
[5] R. Romagnoli, M.C. Deyá, B. del Amo, The mechanism of the anticorrosive action of calcium-exchanged silica, surface coatings international part B: coatings, Transactions 86 (2003) 135–141, https://doi.org/10.1007/BF02699625.
[6] L. Rassouli, R. Naderi, M. Mahdavain, The role of micro/nano zeolites doped with zinc cations in the active protection of epoxy ester coating, Appl. Surf. Sci. 423 (2017) 571–583, https://doi.org/10.1016/j.apsusc.2017.06.245.
[7] H. Yang, W. Li, X. Liu, A. Liu, P. Hang, R. Ding, T. Li, Y. Zhang, W. Wang, C. Xiong, Preparation of corrosion inhibitor loaded zeolites and corrosion resistance of

carbon steel in simulated concrete pore solution, Constr. Build. Mater. 225 (2019) 90–98, https://doi.org/10.1016/j.conbuildmat.2019.07.141.
[8] M.H. Shahini, N. Taheri, H.E. Mohammadloo, B. Ramezanzadeh, A comprehensive overview of nano and micro carriers aiming at curtailing corrosion progression, J. Taiwan Inst. Chem. Eng. 126 (2021) 252–269, https://doi.org/10.1016/j.jtice.2021.06.053.
[9] J.M. Newsam, The zeolite cage structure, Science 231 (1986) 1093–1099.
[10] Y. Zhu, J. Zhuang, Y. Yu, X. Zeng, Research on anti-corrosion property of rare earth inhibitor for X70 steel, J. Rare Earths 31 (2013) 734–740, https://doi.org/10.1016/s1002-0721(12)60350-0.
[11] B.R.W. Hinton, Corrosion inhibition with rare earth metal salts, J. Alloys Comp. 180 (1992) 15–25.
[12] M. Bethencourt, F.J. Botana, J.J. Calvino, M. Marcos, M.A. Rodriguez Chacon, Lanthanide compouds as environmentally friendly corrosion inhibitors of aluminium alloys: a review, corr, Sci. 40 (1998) 1803–1819.
[13] T.D. Manh, P.V. Hien, Q.B. Nguyen, T.N. Quyen, B.R.W. Hinton, N.D. Nam, Corrosion inhibition of steel in naturally-aerated chloride solution by rare-earth 4-hydroxycinnamate compound, J. Taiwan Inst. Chem. Eng. 103 (2019) 177–189, https://doi.org/10.1016/j.jtice.2019.07.012.
[14] H. Wei, J. Tang, X. Chen, Y. Tang, X. Zhao, Y. Zuo, Influence of organic and inorganic cerium salts on the protective performance of epoxy coating, Prog. Org. Coat. 166 (2022), 106763, https://doi.org/10.1016/j.porgcoat.2022.106763.
[15] D. Marunkić, B. Jegdić, J. Pejić, M. Milošević, A. Marinković, B. Radojković, Analysis of inhibitory properties of ce-citrate as a green corrosion inhibitor of low alloy steel in neutral chloride solution, Mater. Corros. (2022), https://doi.org/10.1002/maco.202213079.
[16] B.R.W. Hinton, N.E. Ryan, D.R. Arnott, P. Trathem, L. Wilson, B.E. Williams, The inhibition of aluminum alloy corrosion by rare earth metal cations, Corrosion Australasia 10 (1985) 10–17.
[17] R. Mahmoudi, P. Kardar, A.M. Arabi, R. Amini, P. Pasbakhsh, The active corrosion performance of silane coating treated by praseodymium encapsulated with halloysite nanotubes, Prog. Org. Coat. 138 (2020), 105404, https://doi.org/10.1016/j.porgcoat.2019.105404.
[18] R. Mahmoudi, P. Kardar, A.M. Arabi, R. Amini, P. Pasbakhsh, Acid-modification and praseodymium loading of halloysite nanotubes as a corrosion inhibitor, Appl. Clay Sci. 184 (2020), 105355, https://doi.org/10.1016/j.clay.2019.105355.
[19] O. D'Alessandro, G.J. Selmi, A.R. Di Sarli, R. Romagnoli, C. Deyá, Accelerated tests, a necessary complement of electrochemical assays to evaluate anti-corrosive coatings, J. Appl. Electrochem. 49 (2019) 811–822, https://doi.org/10.1007/s10800-019-01324-z.
[20] S. Roselli, N. Bellotti, C. Deyá, M. Revuelta, B. del Amo, R. Romagnoli, Lanthanum-exchanged zeolite and clay as anticorrosive pigments for galvanized steel, J. Rare Earths 32 (2014) 352–359, https://doi.org/10.1016/s1002-0721(14)60078-8.
[21] S. Roselli, C. Deyá, M. Revuelta, A.R. Di Sarli, R. Romagnoli, Zeolites as reservoirs for Ce(III) as passivating ions in anticorrosion paints, Corros. Rev. 36 (2018) 305–322, https://doi.org/10.1515/corrrev-2017-0090.
[22] O. D'Alessandro, C.E. Byrne, G. Selmi, C. Deyá, Anticorrosive paint with a modified zeolite as functional pigment for SAE 1010 steel protection, Pigment & Resin Technology ahead-of-print (2020), https://doi.org/10.1108/prt-05-2020-0052.
[23] E. Abdullayev, R. Price, D. Shchukin, Y. Lvov, Halloysite tubes as nanocontainers for anticorrosion coating with benzotriazole, ACS Appl. Mater. Interfaces 1 (2009) 1437–1443, https://doi.org/10.1021/am9002028.
[24] D. Fix, D.V. Andreeva, Y.M. Lvov, D.G. Shchukin, H. Möhwald, Application of inhibitor-loaded halloysite nanotubes in active anti-corrosive coatings, Adv. Funct. Mater. 19 (2009) 1720–1727, https://doi.org/10.1002/adfm.200800946.
[25] Y.M. Lvov, D.G. Shchukin, H. Mohwald, Halloysite clay nanotubes for controlled release of protective agents, ACS Nano 2 (2008) 814–820.
[26] E. Shchukina, D. Grigoriev, T. Sviridova, D. Shchukin, Comparative study of the effect of halloysite nanocontainers on autonomic corrosion protection of polyepoxy coatings on steel by salt-spray tests, Prog. Org.Coat. 108 (2017) 84–89, https://doi.org/10.1016/j.porgcoat.2017.03.018.
[27] P. Yuan, P.D. Southon, Z. Liu, M.E.R. Green, J.M. Hook, S.J. Antill, C.J. Kepert, Functionalization of halloysite clay nanotubes by grafting with γ-aminopropyltriethoxysilane, J. Phys. Chem. C 112 (2008) 15742–15751.
[28] T.F. Bates, F.A. Hildebrand, A. Swineford, Morphology and structure of endellite and halloysite, The American Mineralogist 35 (1950).
[29] F. Cravero, L. Fernández, S. Marfil, M. Sánchez, P. Maiza, A. Martínez, Spheroidal halloysites from Patagonia, argentina: some aspects of their formation and applications, Appl. Clay Sci. 131 (2016) 48–58, https://doi.org/10.1016/j.clay.2016.01.011.
[30] A. Khan, A. Hassanein, S. Habib, M. Nawaz, R.A. Shakoor, R. Kahraman, Hybrid halloysite nanotubes as smart carriers for corrosion protection, ACS Appl. Mater. Interfaces 12 (2020) 37571–37584, https://doi.org/10.1021/acsami.0c08953.
[31] A. Gautam, T. Siva, S. Sathiyanarayanan, K.V. Gobi, R. Subasri, Capped inhibitor-loaded halloysite nanoclay-based self-healing silica coatings for corrosion protection of mild steel, Ceram. Int. 48 (2022) 30151–30163, https://doi.org/10.1016/j.ceramint.2022.06.288.
[32] S. Manasa, A. Jyothirmayi, T. Siva, B.V. Sarada, M. Ramakrishna, S. Sathiyanarayanan, K.V. Gobi, R. Subasri, Nanoclay-based self-healing, corrosion protection coatings on aluminum, A356.0 and AZ91 substrates, J. Coat. Technol. Res. 14 (2017) 1195–1208, https://doi.org/10.1007/s11998-016-9912-3.
[33] S. Manasa, A. Jyothirmayi, T. Siva, S. Sathiyanarayanan, K.V. Gobi, R. Subasri, Effect of inhibitor loading into nanocontainer additives of self-healing corrosion protection coatings on aluminum alloy A356.0, J. Alloys Compd. 726 (2017) 969–977, https://doi.org/10.1016/j.jallcom.2017.08.037.
[34] S.H. Adsul, U.D. Bagale, S.H. Sonawane, R. Subasri, Release rate kinetics of corrosion inhibitor loaded halloysite nanotube-based anticorrosion coatings on magnesium alloy AZ91D, J. Magnesium and Alloys 9 (2021) 202–215, https://doi.org/10.1016/j.jma.2020.06.010.
[35] F. Cravero, A.M. Gabriel, F. Pestalardo, Halloysite deposits in mamil choique, province of Río Negro, Patagonia, Revista de la Asociacion Geologica Argentina 65 (2009) 586–592.
[36] F. Cravero, P.J. Maiza, S.A. Marfil, Halloysite in argentinian deposits: origin and textural constraints, Clay Miner. 47 (2018) 329–340, https://doi.org/10.1180/claymin.2012.047.3.04.
[37] J.I. Drever, The preparation of oriented clay mineral specimens for X-ray diffraction analysis by a filte-membrane peel technique, Am. Mineral. 58 (1973) 553–554.
[38] F.J. Welcher, Organic analytical reagents, van Nostrand, D., New York, USA, 1947.
[39] N. Danyliuk, J. Tomaszewska, T. Tatarchuk, Halloysite nanotubes and halloysite-based composites for environmental and biomedical applications, J. Mol. Liq. 309 (2020), 113077, https://doi.org/10.1016/j.molliq.2020.113077.
[40] Y. Zhang, Y. Li, Y. Zhang, Preparation and intercalation structure model of halloysite-stearic acid intercalation compound, Appl. Clay Sci. 187 (2020), 105451, https://doi.org/10.1016/j.clay.2020.105451.
[41] A.M. Carrillo, C.M. Urruchurto, J.G. Carriazo, S. Moreno, R.A. Molina, Structural and textural characterization of a colombian halloysite, Revista Mexicana de Ingeniería Química 13 (2014) 563–571.
[42] E. Joussein, S. Petit, J. Churchman, B. Theng, D. Righi, B. Delvaux, Halloysite clay minerals- a review, Clay Miner. 40 (2005) 383–426.
[43] S. Eskandari, R. Stephenson, I. Toth, Current boundaries in the formulation of lipid based delivery systems, Eds, in: A. Samad, S. Beg, I. Nazish (Eds.), Liposomal delivery systems: advances and challenges Future science, 2016, pp. 160–174.
[44] Y. Lvov, E. Abdullayev, Functional polymer–clay nanotube composites with sustained release of chemical agents, Prog. Polym. Sci. 38 (2013) 1690–1719, https://doi.org/10.1016/j.progpolymsci.2013.05.009.
[45] E. Abdullayev, Y. Lvov, Halloysite clay nanotubes as a ceramic "skeleton" for functional biopolymer composites with sustained drug release, J. Mater. Chem. B 1 (2013) 2894–2903, https://doi.org/10.1039/c3tb20059k.
[46] F.H. Firschlng, S.N. Brune, Solubility products of the trivalent rare-earth phosphates, J. Chem. Eng. Data 36 (1991) 93–95.
[47] C. Deyá, B. del Amo, R. Romagnoli, Ceramic microspheres to improve anticorrosive performance of phosphate paints, Ceram. Int. 38 (2012) 2637–2646, https://doi.org/10.1016/j.ceramint.2011.11.029.